

FIELD REVERSED CONFIGURATION FORMATION SIMULATIONS WITH MACH2

George J. Marklin and Michael H. Frese

**Prime Contractor
Maxwell Technologies, Inc.
2501 Yale SE, Ste. 300
Albuquerque, NM 87106**

**Subcontractor
NumerEx
2309 Renard SE, Suite 220
Albuquerque, NM 87106**

December 2000

FINAL REPORT

APPROVED FOR PUBLIC RELEASE; DISTRIBUTION IS UNLIMITED.



**AIR FORCE RESEARCH LABORATORY
Directed Energy Directorate
3550 Aberdeen Ave SE
AIR FORCE MATERIEL COMMAND
KIRTLAND AIR FORCE BASE, NM 87117-5776**

20010424 062

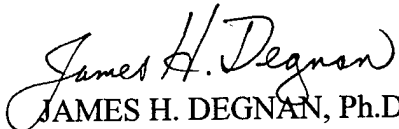
Using Government drawings, specifications, or other data included in this document for any purpose other than Government procurement does not in any way obligate the U.S. Government. The fact that the Government formulated or supplied the drawings, specifications, or other data, does not license the holder or any other person or corporation; or convey any rights or permission to manufacture, use, or sell any patented invention that may relate to them.

This report has been reviewed by the Public Affairs Office and is releasable to the National Technical Information Service (NTIS). At NTIS, it will be available to the general public, including foreign nationals.

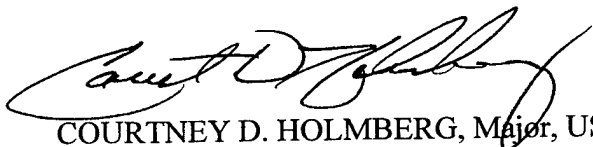
If you change your address, wish to be removed from this mailing list, or your organization no longer employs the addressee, please notify AFRL/DEHP, 3550 Aberdeen Ave SE, Kirtland AFB, NM 87117-5776.


Do not return copies of this report unless contractual obligations or notice on a specific document requires its return.

This report has been approved for publication.


JAMES H. DEGNAN, Ph.D, DR-VI
Project Manager

FOR THE COMMANDER


COURTNEY D. HOLMBERG, Major, USAF
Chief, High Power Microwave Division


R. EARL GOOD, SES
Director, Directed Energy

REPORT DOCUMENTATION PAGE			Form Approved OMB No. 074-0188	
Public reporting burden for this collection of information is estimated to average 1 hour per response, including the time for reviewing instructions, searching existing data sources, gathering and maintaining the data needed, and completing and reviewing this collection of information. Send comments regarding this burden estimate or any other aspect of this collection of information, including suggestions for reducing this burden to Washington Headquarters Services, Directorate for Information Operations and Reports, 1215 Jefferson Davis Highway, Suite 1204, Arlington, VA 22202-4302, and to the Office of Management and Budget, Paperwork Reduction Project (0704-0188), Washington, DC 20503				
1. AGENCY USE ONLY (Leave blank)	2. REPORT DATE Dec 2000	3. REPORT TYPE AND DATES COVERED Final Report; 16 May to 30 Nov 2000		
4. TITLE AND SUBTITLE Field Reversed Configuration Formation Simulations With MACH2		5. FUNDING NUMBERS F29601-00-D-0055 PE: 62601F PR: 5797 TA: HE WU: 01		
6. AUTHOR(S) George J. Marklin and Michael H. Frese				
7. PERFORMING ORGANIZATION NAME(S) AND ADDRESS(ES) Prime Contractor Maxwell Technologies, Inc. 2501 Yale SE Ste 300 Albuquerque, NM 87106 Subcontractor Numerex 2309 Renard SE, Suite 220 Albuquerque, NM 87106		8. PERFORMING ORGANIZATION REPORT NUMBER		
9. SPONSORING / MONITORING AGENCY NAME(S) AND ADDRESS(ES) Air Force Research Laboratory / DEHP 3550 Aberdeen Ave, SE Kirtland Air Force Base, NM 87117-5776		10. SPONSORING / MONITORING AGENCY REPORT NUMBER AFRL-DE-TR-2001-1001		
11. SUPPLEMENTARY NOTES				
12a. DISTRIBUTION / AVAILABILITY STATEMENT Approved for Public Release; Distribution is Unlimited.			12b. DISTRIBUTION CODE	
13. ABSTRACT (<i>Maximum 200 Words</i>) A Field Reversed Configuration (FRC) plasma is formed by applying a modest magnetic bias field to a gas, then ionizing the gas, and quickly applying a larger field of opposite polarity. The theta pinch that results can produce a magnetically insulated plasma of hundreds of electron volts in temperature. Simulations of this experiment can now be performed using the 2 1/2-dimensional magnetohydrodynamic (MHD) code MACH2. This report describes the modifications to the code employed and simulations performed to test the model that explores three different anomalous resistivity models and three different initial densities for one of those models.				
14. SUBJECT TERMS Shiva, liner implosion, solid dielectric, field reversed configuration (FRC), MACH2			15. NUMBER OF PAGES 22	
			16. PRICE CODE	
17. SECURITY CLASSIFICATION OF REPORT UNCLASSIFIED	18. SECURITY CLASSIFICATION OF THIS PAGE UNCLASSIFIED	19. SECURITY CLASSIFICATION OF ABSTRACT UNCLASSIFIED	20. LIMITATION OF ABSTRACT UNLIMITED	

CONTENTS

Figures	iv
1.0 Introduction	1
2.0 Code Modifications	1
3.0 Simulation Results	3
4.0 Conclusion.....	15

FIGURES

<u>Figure</u>	<u>Page</u>
1. Flux Plot Showing Initial Bias Field at $t = 0$	4
2. Flux and Density Plots at $t = 0.5 \mu s$ for the Chodura Model with $n_i = 6.7 \times 10^{15}$	5
3. Flux and Density Plots at $t = 1.0 \mu s$ for the Chodura Model with $n_i = 6.7 \times 10^{15}$	6
4. Flux and Density Plots at $t = 1.5 \mu s$ for the Chodura Model with $n_i = 6.7 \times 10^{15}$	6
5. Flux and Density Plots at $t = 2.0 \mu s$ for the Chodura Model with $n_i = 6.7 \times 10^{15}$	6
6. Flux and Density Plots at $t = 2.5 \mu s$ for the Chodura Model with $n_i = 6.7 \times 10^{15}$	7
7. Flux and Density Plots at $t = 3.0 \mu s$ for the Chodura Model with $n_i = 6.7 \times 10^{15}$	7
8. Flux and Density Plots at $t = 3.5 \mu s$ for the Chodura Model with $n_i = 6.7 \times 10^{15}$	7
9. Flux and Density Plots at $t = 4.0 \mu s$ for the Chodura Model with $n_i = 6.7 \times 10^{15}$	8
10. Flux and Density Plots at $t = 4.5 \mu s$ for the Chodura Model with $n_i = 6.7 \times 10^{15}$	8
11. Flux and Density Plots at $t = 5.0 \mu s$ for the Chodura Model with $n_i = 6.7 \times 10^{15}$	8
12. Flux and Density Plots at $t = 3.0 \mu s$ for the Ohmic-cutoff model with $n_i = 6.7 \times 10^{15}$	9
13. Flux and Density Plots at $t = 3.0 \mu s$ for the Lower Hybrid Model with $n_i = 6.7 \times 10^{15}$	9
14. Flux and Density Plots at $t = 3.0 \mu s$ for the Chodura Model with $n_i = 6.7 \times 10^{15}$	10
15. Peak density Time Histories for Three Anomalous Resistivity Models, All with $n_i = 6.7 \times 10^{15}$	10
16. Flux and Density Plots at $t = 3.0 \mu s$ for the Chodura Model with $n_i = 3.3 \times 10^{15}$	11
17. Flux and Density Plots at $t = 3.0 \mu s$ for the Chodura Model with $n_i = 1.7 \times 10^{15}$	11
18. Peak Density Time Histories for the Chodura Model, $n_i = 6.7 \times 10^{15}$, 3.3×10^{15} , 1.7×10^{15}	12
19. Temperature Plot at $t = 3.0 \mu s$ for the Ohmic-Cutoff Model with $n_i = 6.7 \times 10^{15}$	13
20. Temperature Plot at $t = 3.0 \mu s$ for the Lower Hybrid Model with $n_i = 6.7 \times 10^{15}$	13
21. Temperature Plot at $t = 3.0 \mu s$ for the Chodura Model with $n_i = 6.7 \times 10^{15}$	13
22. Temperature Plot at $t = 3.0 \mu s$ for the Chodura Model with $n_i = 3.3 \times 10^{15}$	14
23. Temperature Plot at $t = 3.0 \mu s$ for the Chodura Model with $n_i = 1.7 \times 10^{15}$	14

1.0

INTRODUCTION

An FRC formation experiment could provide a test bed for ionization kinetics models since neutral species can propagate easily across field lines, but ionized species can not. Thus, the depth of penetration of the ionized species, as identified by spectral methods, is a useful diagnostic for determining the validity of such models.

This report describes work by NumerEx to simulate the formation of an FRC using MACH2. The goal was only to demonstrate the capability of doing the simulations, not to simulate any actual experimental configuration. Some very general details of a possible experimental configuration were inferred from the proposal: "Magnetized Target Fusion - A Proof-of-principle Research Proposal" by K.F. Shoenberg and R.E. Siemon [LA-UR-98-2413]. This proposal describes an experimental program to investigate the feasibility of Magnetized Target Fusion (MTF) by liner implosion of an FRC target. The first phase of this project, the formation of the FRC, will be carried out at Los Alamos National Laboratory. MACH2 is the primary tool used for MHD simulation at AFRL; however, the traditional kinds of problems for which MACH2 is well adapted to solving do not include inductively-driven formation schemes of the type that will be used for the FRC. NumerEx has completed work on adapting the code to solve this new class of problems. Section II will briefly describe the modifications that were made to MACH2 and explain how its capabilities have been extended. Section III will show some preliminary results from simulations of FRC formation based on a sample configuration created to roughly match the examples shown in the above mentioned proposal.

2.0

CODE MODIFICATIONS

It has been difficult to simulate configurations where the plasma current is driven inductively by time-varying externally applied vacuum fields with MACH2. The problem manifests itself in the vacuum region between the plasma and the applied field. If the vacuum region is modeled as high resistivity plasma, the magnetic field solver may diverge there, but if the resistivity is not

set high enough then the electric field cannot penetrate into the plasma where it is needed to drive the current.

The problem was solved by rewriting the diffusion solver to use the flux function, $\psi \equiv rA_\theta$, in place of the in-plane components of the magnetic field. These field components are then defined in terms of the flux function by taking the curl:

$$\mathbf{B} = \nabla \times \mathbf{A}_\theta = \nabla \psi \times \hat{\theta} / r \quad (0.1)$$

with the unit vector in the out-of-plane direction. Hence, the field diffusion equation

$$\frac{\partial \mathbf{B}}{\partial t} = -\nabla \times \eta \nabla \times \mathbf{B} \quad (0.2)$$

is replaced by the flux diffusion equation

$$\frac{\partial \psi}{\partial t} = \eta r^2 \nabla \cdot r^{-2} \nabla \psi. \quad (0.3)$$

This has two important advantages. First, since the resistivity only appears outside the differential operator, it can be divided out, leading to

$$\sigma \frac{\partial \psi}{\partial t} = r^2 \nabla \cdot r^{-2} \nabla \psi \quad (0.4)$$

Since only the conductivity need be specified, it can be set equal to zero in the vacuum region, making the resistivity infinite there. This is the equation that the new code solves with a fully implicit Euler step. The conjugate gradient method is used to solve the implicit equations. The multi-grid solvers used elsewhere in the code might be more efficient but they are too complex to have been rewritten in the time allowed for this project.

The second important advantage of using the flux function is that the magnetic field is automatically divergence free because it is defined as the curl of a vector potential. This property can be reproduced in the numerical equations if the finite volume difference operators satisfy $\text{div}(\text{curl})=0$. The original operators in MACH2 did not satisfy this exactly, but it was found

that they could be made to do so, by changing the geometry coefficients from which they are computed. The version of the code used for the simulations described here maintains $\text{div}(\mathbf{B})=0$ exactly. An explanation of how this is done will be written up and submitted for publication at a later time.

The Lagrangian hydro step in MACH2 does not have to be altered because that step must conserve flux on physical grounds; hence, the flux function does not change across it. This observation makes it possible to retain the implicit hydro step and its stabilizing iteration on the magnetic field, yet discard the resulting magnetic field in favor of the flux function at the *beginning* of the iteration. The magnetic field advection is then replaced by advection of the flux function itself.

MACH2 now has the capability of simulating problems with any kind of time-varying vacuum field and can do pure vacuum field diffusion calculations of the type that were formerly done using the D code¹.

3.0

SIMULATION RESULTS

Magnetic Fields The formation scheme simulation uses a 20 cm long, 6 cm radius main field coil and two 5 cm long, 6 cm radius cusp coils at each end of the main coil, but separated from it by 5 cm long insulating gaps. The configuration is symmetric about the mid-plane and only the left half is shown in all the plots. The simulation included the complete device and both halves remained symmetric. The flux in each coil is specified as a function of time to be a linear ramp up to 3 μs and constant thereafter. This corresponds to a square wave voltage pulse lasting 3 μs . Of course, any waveform could have been specified, or the external circuit could have been specified and the voltage computed self-consistently. The flux scheme does not permit direct specification of the current in the coils. Rather, it must be determined from the simulation by integration. The flux values are set so that the initial reversed bias field is -4.7 kG and it swings to +33 kG in 3 μs (with no FRC present—it is higher with the FRC because the same flux is compressed into a smaller area). The cusp field starts at 5.6 kG and swings to 40 kG in the same

3 μ s. The cusp field is always slightly higher than the main field to confine the FRC. Figure 1 shows the coil geometry and the initial bias field. The dimensions are in meters. The right edge of the plot is the mid-plane and the left edge is one end. Symmetry boundary conditions are used for the field at the ends.

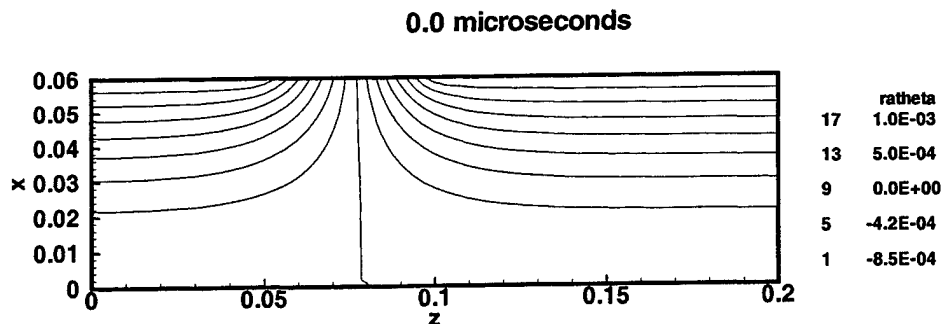


Figure 1. Flux Plot Showing Initial Bias Field at $t = 0$.

Physical Model The physical model consists of magnetic diffusion, magnetohydrodynamics, anisotropic thermal diffusion, and radiation cooling by emission. Mass is allowed to flow out through the ends and the single-temperature energy equation includes Ohmic heating, radiation losses and anisotropic thermal conduction with thermal boundaries treated as heat sinks held at 1 eV. The initial mass density is $2 \times 10^{-5} \text{ kg/m}^3$ of deuterium for most of the runs described here. This corresponds to an initial ion number density of $6.7 \times 10^{15} \text{ cm}^{-3}$. One run uses half this value and another uses a quarter. The initial temperature is always 1 eV.

Anomalous Resistivity Spitzer resistivity is never adequate for this type of simulation because it invariably leads to hot, highly conducting vacuum regions which prevent electric fields from diffusing into the plasma. Some type of anomalous resistivity model is needed to prevent low density regions from becoming highly conductive. Unfortunately, the state of the art in anomalous resistivity theory has not developed to the point where any particular model is known to be applicable to a given situation. The only guidance available is to look for past experiments where some empirical information may have been acquired. Past FRC experiments at LANL

¹ DT—A Magnetic Diffusion Code with Ohmic Heating and Thermal Conduction for Arbitrary

have shown that the Chodura model with empirically determined parameters has led to some agreement with simulation² so this model, with their parameters, was used for this simulation. Three runs were done using this model, with three different initial densities. One run was also done using the lower hybrid model with MACH2's default parameters and one run was done with Spitzer, but with the Ohmic heating turned off in regions with density less than $5 \times 10^{14} \text{ cm}^{-3}$.

Discussion and Conclusions Figures 2 through 11 are flux and number density contour plots showing the time evolution of an FRC formation simulation using the Chodura model with initial density $n_i = 6.7 \times 10^{15}$.

The contour line that goes to $r = 0$ is $\phi = 0$, and the region it encloses to the lower right has negative flux values. Note that the flux contour interval is much smaller for negative values than for positive. Other simulations with the different anomalous resistivity models and the different initial densities look very similar with only slight differences in the size of the FRC.

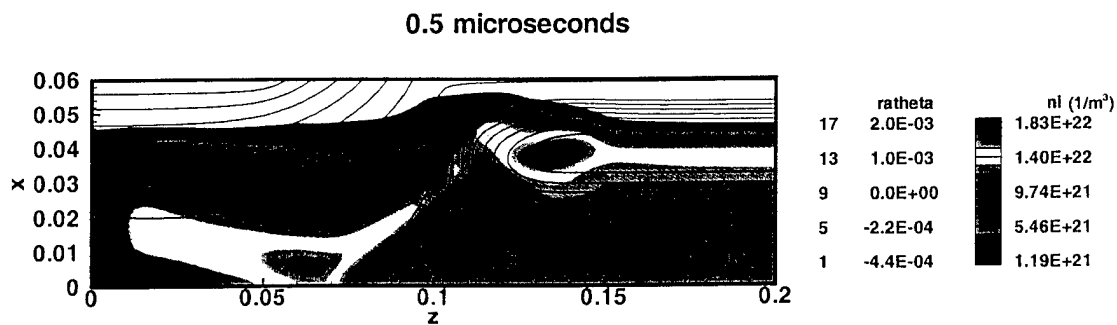


Figure 2. Flux and Density Plots at $t = 0.5 \mu\text{s}$ for the Chodura Model with $n_i = 6.7 \times 10^{15}$.

Axisymmetric Geometries; George Marklin; NumerEx 97-02.

² Brackbill and Milroy; Physics of Fluids; May 1982

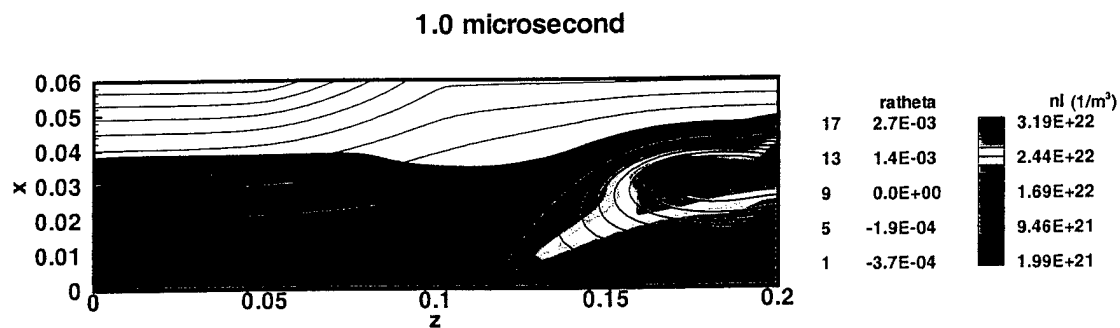


Figure 3. Flux and Density Plots at $t = 1.0 \mu\text{s}$ for the Chodura Model with $n_i = 6.7 \times 10^{15}$.

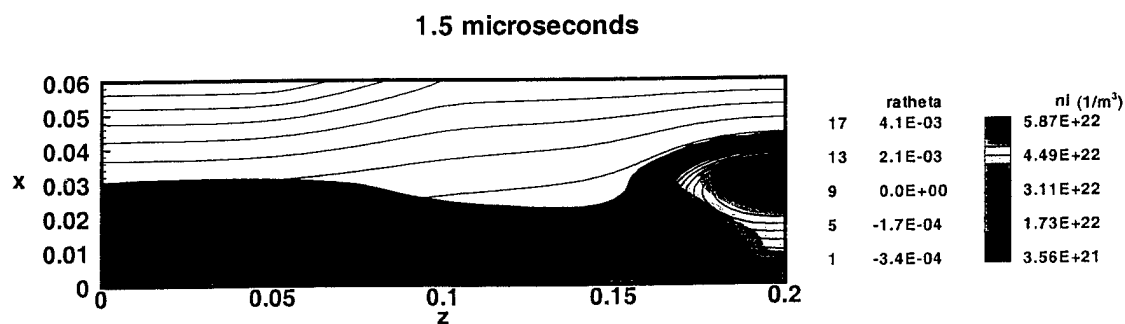


Figure 4. Flux and Density Plots at $t = 1.5 \mu\text{s}$ for the Chodura Model with $n_i = 6.7 \times 10^{15}$.

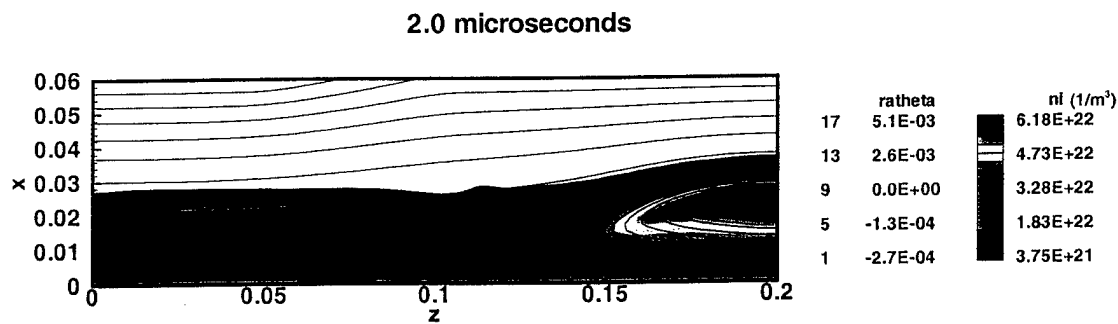


Figure 5. Flux and Density Plots at $t = 2.0 \mu\text{s}$ for the Chodura Model with $n_i = 6.7 \times 10^{15}$.

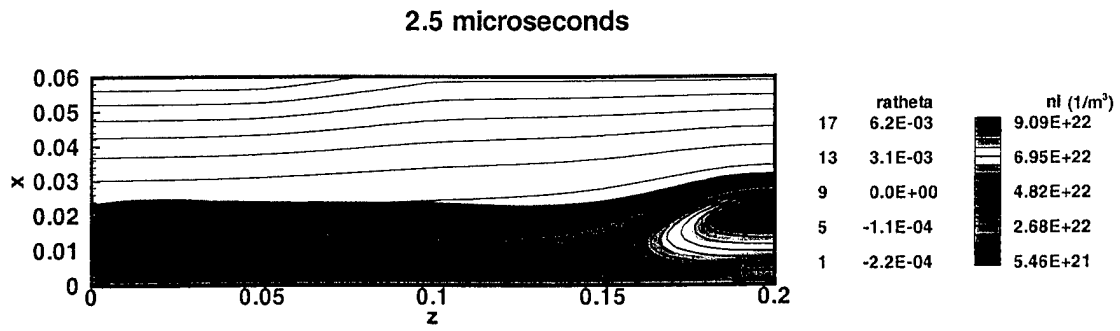


Figure 6. Flux and Density Plots at $t = 2.5 \mu\text{s}$ for the Chodura Model with $n_i = 6.7 \times 10^{15}$.

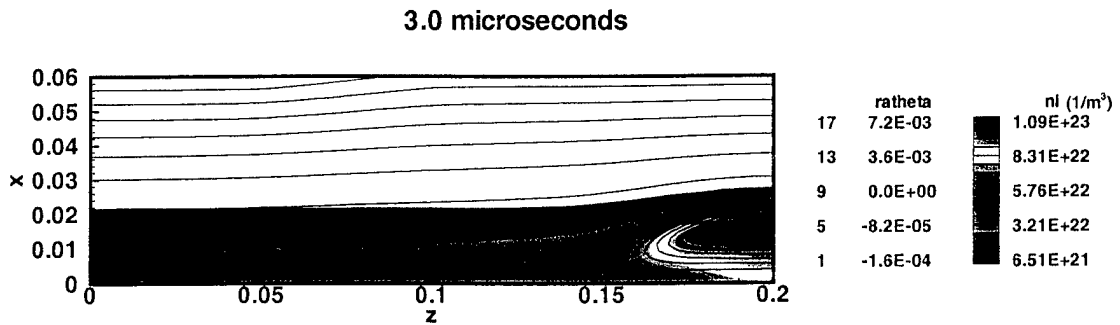


Figure 7. Flux and Density Plots at $t = 3.0 \mu\text{s}$ for the Chodura Model with $n_i = 6.7 \times 10^{15}$.

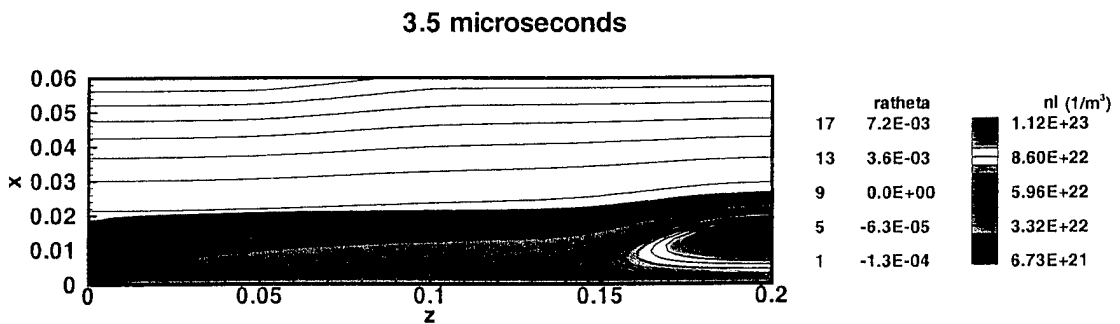


Figure 8. Flux and Density Plots at $t = 3.5 \mu\text{s}$ for the Chodura Model with $n_i = 6.7 \times 10^{15}$.

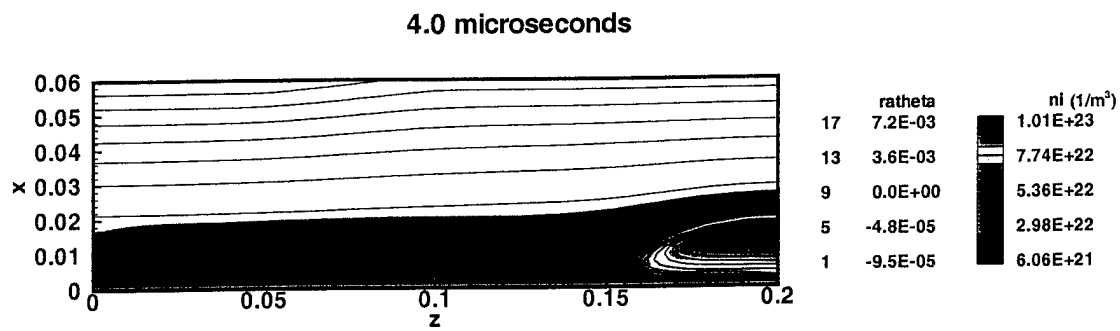


Figure 9. Flux and Density Plots at $t = 4.0 \mu\text{s}$ for the Chodura Model with $n_i = 6.7 \times 10^{15}$.

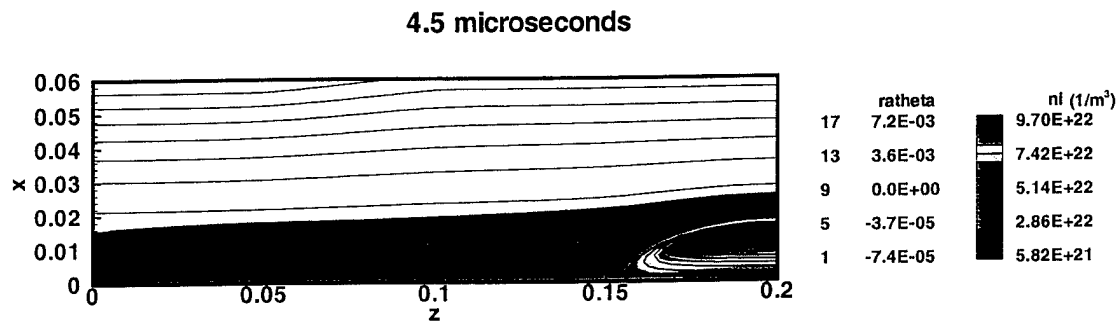


Figure 10. Flux and Density Plots at $t = 4.5 \mu\text{s}$ for the Chodura Model with $n_i = 6.7 \times 10^{15}$.

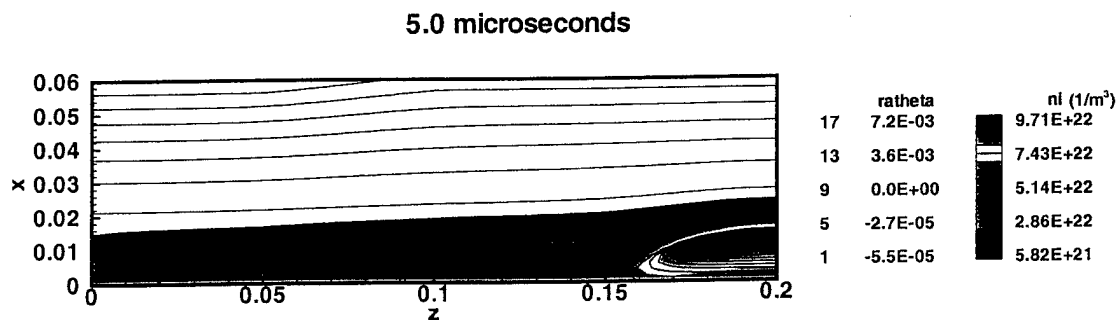


Figure 11. Flux and Density Plots at $t = 5.0 \mu\text{s}$ for the Chodura Model with $n_i = 6.7 \times 10^{15}$.

There are significant differences, however, in the peak densities and in the temperatures. Figures 12, 13 and 14 show results from the three different anomalous resistivity models at $3 \mu\text{s}$. Compare the Ohmic-cutoff model in Figure 12 to the Chodura in Figure 14 and notice the smaller size and 60% higher density. Figure 13 shows the lower hybrid model at $3 \mu\text{s}$; compare

this to Figure 14 and notice the intermediate size and density. The dependence of the density on the choice of anomalous resistivity model is most clearly seen in Figure 15 which shows a time history of the peak density in the three different models. Note the differences in the equilibrium density levels after $3 \mu\text{s}$ and the collapse in density after $8 \mu\text{s}$ for the Chodura model only. These variations limit the confidence that can be placed on any density prediction.

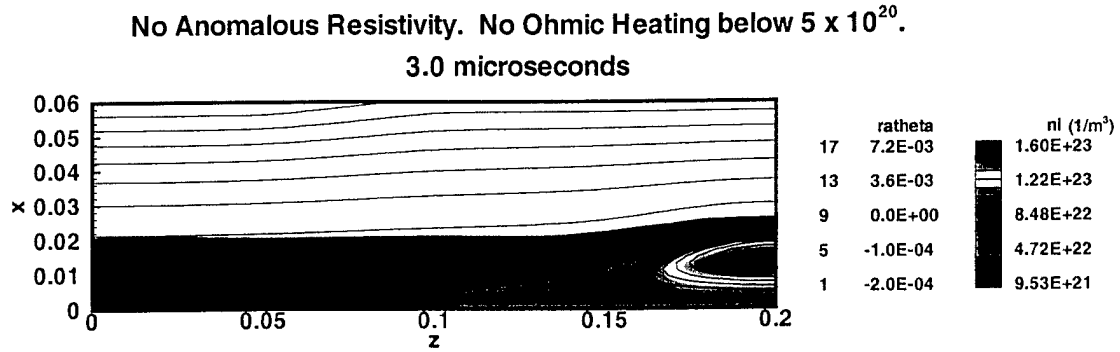


Figure 12. Flux and Density Plots at $t = 3.0 \mu\text{s}$ for the Ohmic-cutoff model with $n_i = 6.7 \times 10^{15}$.

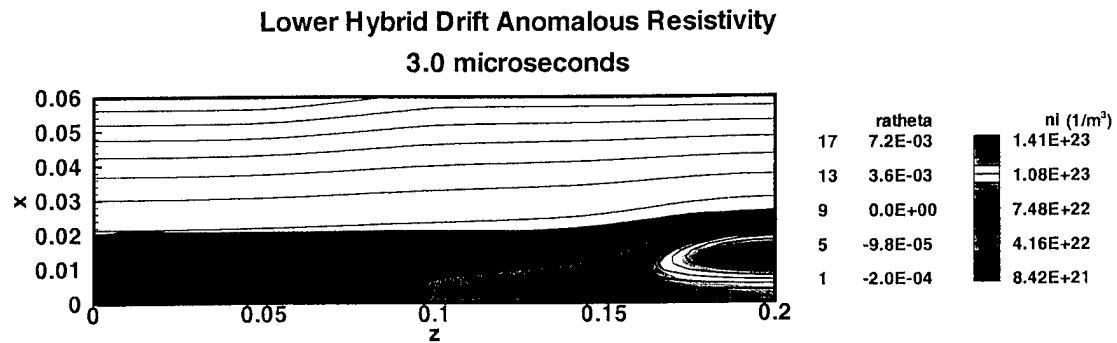


Figure 13. Flux and Density Plots at $t = 3.0 \mu\text{s}$ for the Lower Hybrid Model with $n_i = 6.7 \times 10^{15}$.

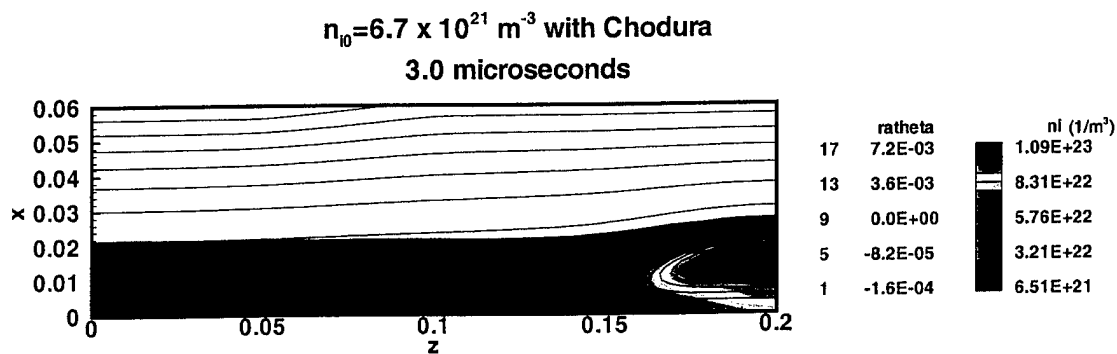


Figure 14. Flux and Density Plots at $t = 3.0 \mu\text{s}$ for the Chodura Model with $n_i = 6.7 \times 10^{15}$.

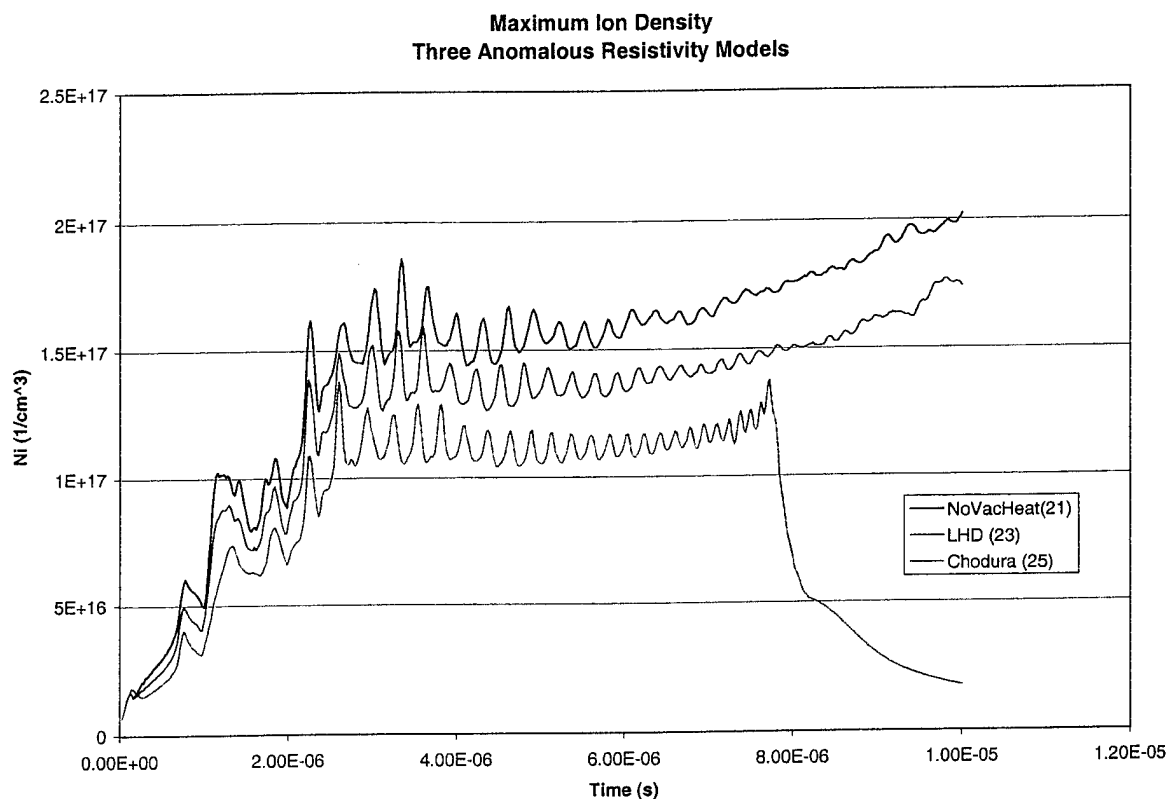


Figure 15. Peak density Time Histories for Three Anomalous Resistivity Models, All with $n_i = 6.7 \times 10^{15}$.

Figures 16 and 17 show results at $3 \mu\text{s}$ from runs using the Chodura model with different initial density. They look very similar except for a slightly smaller size for the lower densities. Figure 18 shows the time history of the peak density in these three cases. The ratios of the equilibrium

densities follow the ratios of the initial values but the density collapse occurs much sooner at the lower densities. The physics of this density collapse has not been investigated.

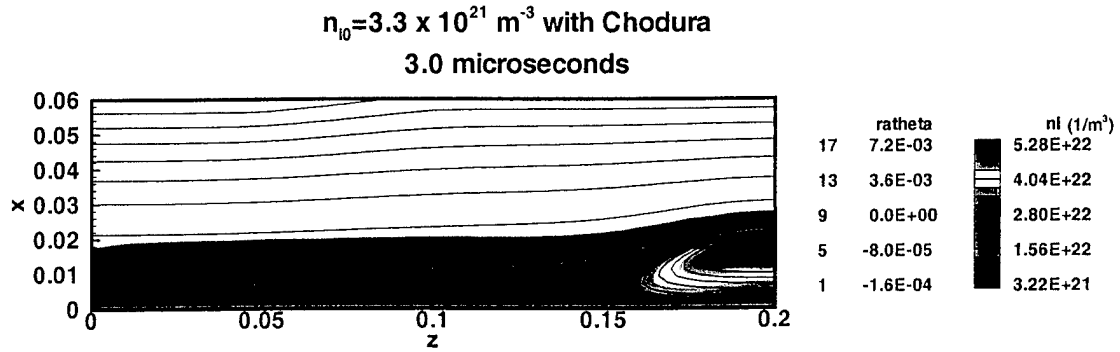


Figure 16. Flux and Density Plots at $t = 3.0 \mu\text{s}$ for the Chodura Model with $n_i = 3.3 \times 10^{15}$.

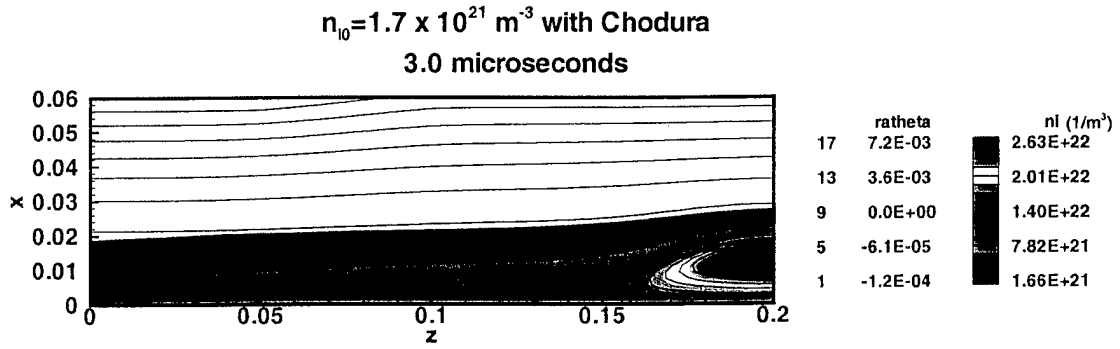


Figure 17. Flux and Density Plots at $t = 3.0 \mu\text{s}$ for the Chodura Model with $n_i = 1.7 \times 10^{15}$.

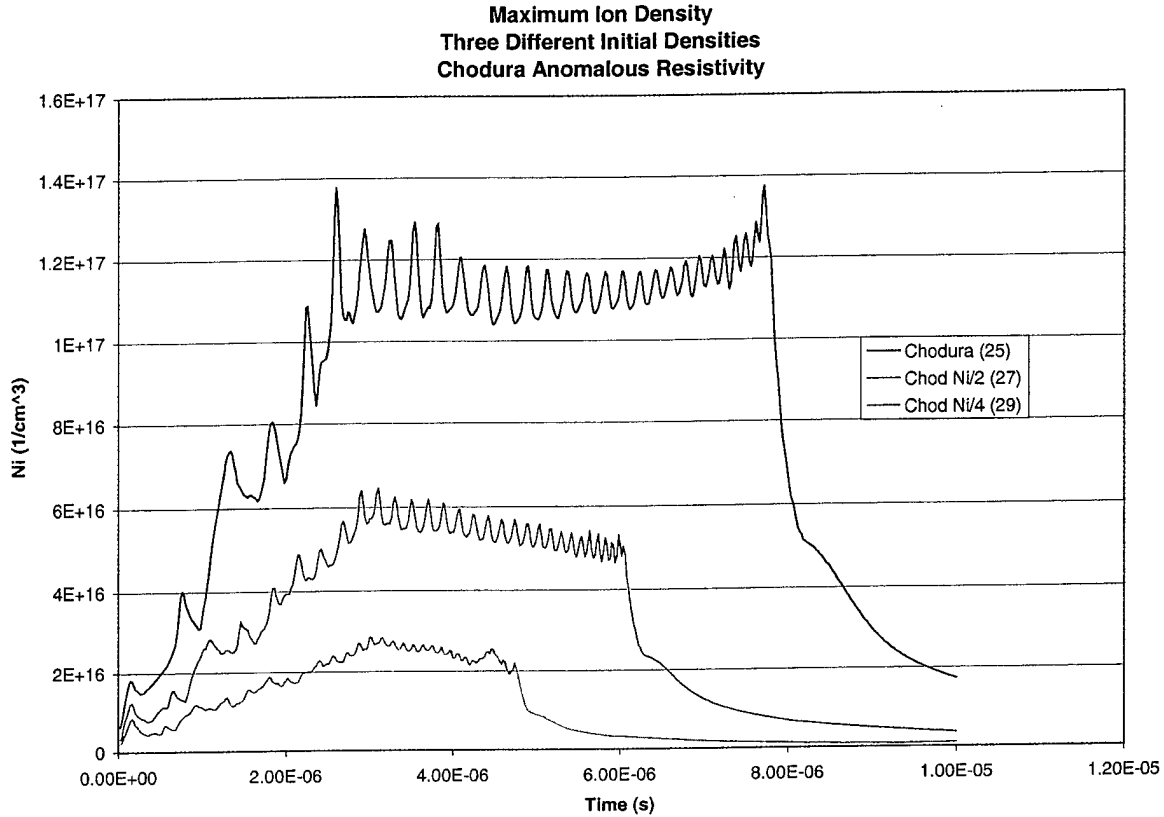


Figure 18. Peak Density Time Histories for the Chodura Model, $n_i = 6.7 \times 10^{15}$, 3.3×10^{15} , 1.7×10^{15} .

Figures 19, 20 and 21 show temperature plots for each of the three different anomalous resistivity models, all with the same initial density. They are all about the same in the FRC interior, ranging from around 200 eV for the Chodura and lower hybrid models, down to 150 eV for the Ohmic-cutoff model.

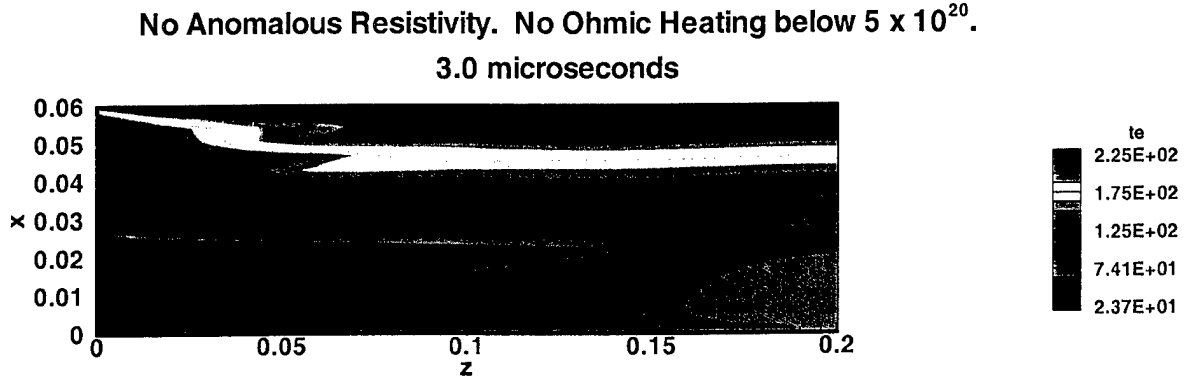


Figure 19. Temperature Plot at $t = 3.0 \mu s$ for the Ohmic-Cutoff Model with $n_i = 6.7 \times 10^{15}$.

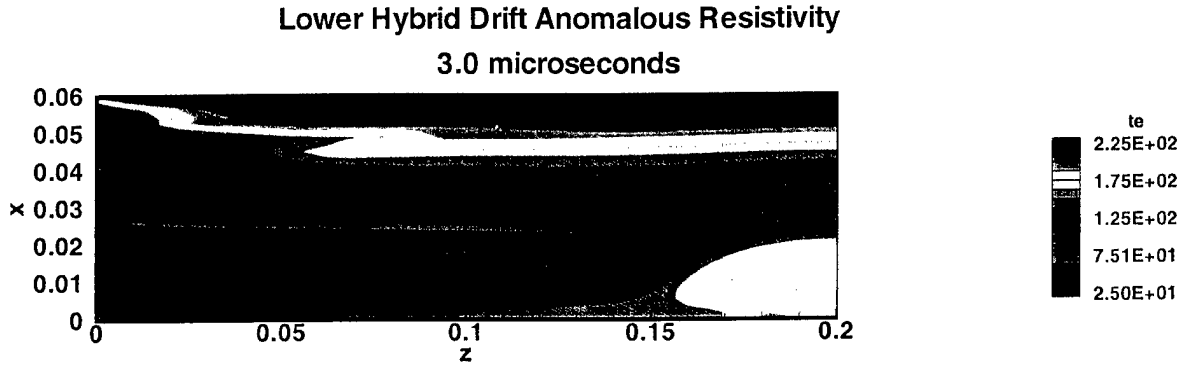


Figure 20. Temperature Plot at $t = 3.0 \mu s$ for the Lower Hybrid Model with $n_i = 6.7 \times 10^{15}$.

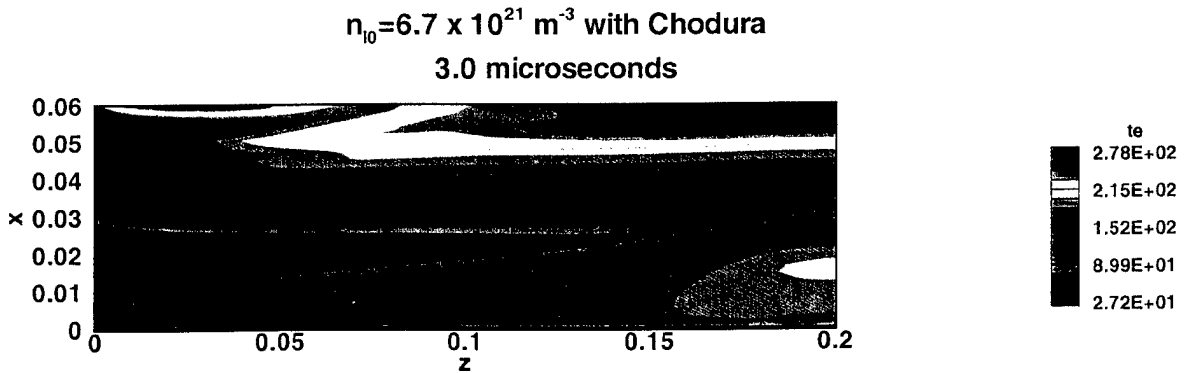


Figure 21. Temperature Plot at $t = 3.0 \mu s$ for the Chodura Model with $n_i = 6.7 \times 10^{15}$.

Figures 21, 22 and 23 show temperature plots for the Chodura model at three different initial densities. The temperature of the FRC increases by about the same ratio as the density drops: 200 eV to 400 eV to 800 eV. This makes the pressure about the same for each case, which it

must be because in equilibrium it is balanced by the magnetic field pressure, which is the same. The hottest FRC decays the fastest – because of the density dependence in the anomalous resistivity – if these results can be believed. The question of whether this anomalous resistivity will be applicable to any experiment cannot be answered until the experiment is carried out.

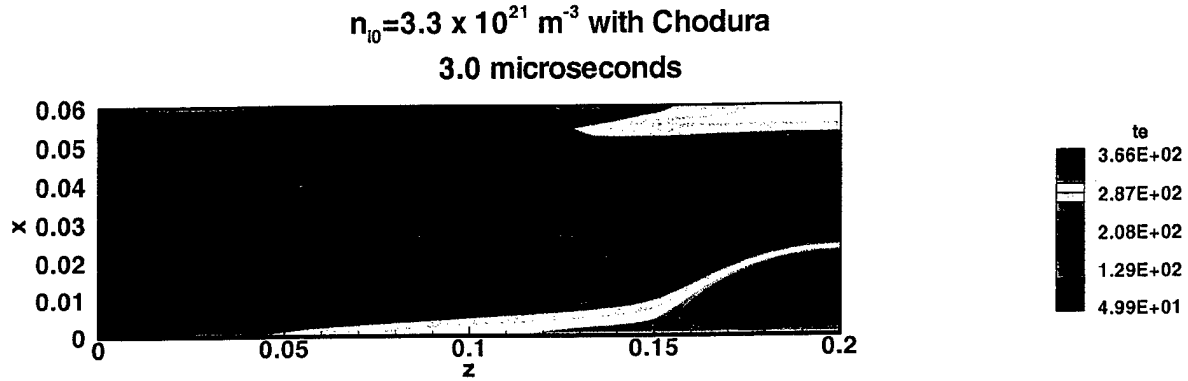


Figure 22. Temperature Plot at $t = 3.0 \mu\text{s}$ for the Chodura Model with $n_i = 3.3 \times 10^{15}$.

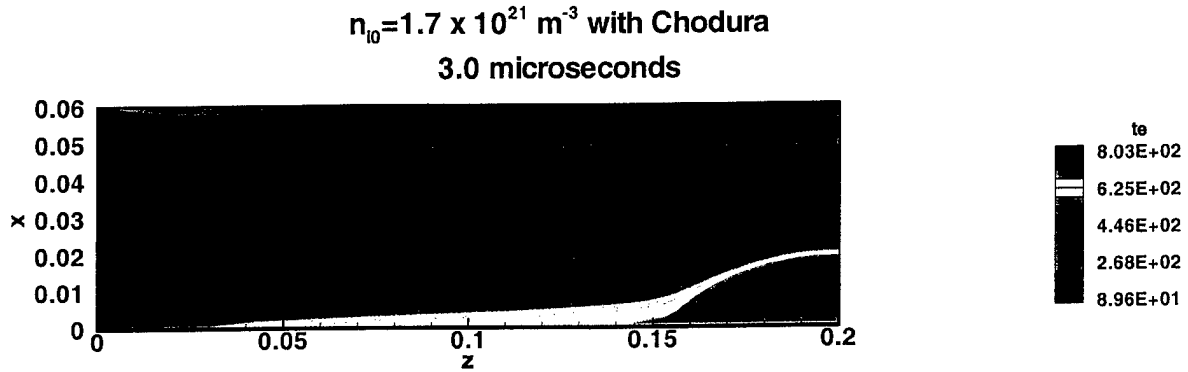


Figure 23. Temperature Plot at $t = 3.0 \mu\text{s}$ for the Chodura Model with $n_i = 1.7 \times 10^{15}$.

4.0

CONCLUSION

Simulations of FRC formation experiments can now be performed using the 2½-dimensional magnetohydrodynamic code MACH2. This report describes the modifications to the code employed and simulations performed to test the model that explore three different anomalous resistivity models and three different initial densities for one of those models. The maximum density and temperature depend weakly on the resistivity model, and strongly on the initial density.

DISTRIBUTION LIST

DTIC/OCP 8725 John J. Kingman Rd, Suite 0944 Ft Belvoir, VA 22060-6218	1 cy
AFSAA/SAMI 1570 Air Force Pentagon Washington, DC 20330-1570	1 cy
AFRL/VSIL Kirtland AFB, NM 87117-5776	2 cys
AFRL/VSIH Kirtland AFB, NM 87117-5776	1 cy
Maxwell Technologies, Inc. 2501 Yale SE, Ste. 300 Albuquerque, NM 87106	1 cy
NumerEx 2309 Renard SE, Ste 220 Albuquerque, NM 87106	1 cy
Official Record Copy AFRL/DEHP/James H Degnan, PH.D 3550 Aberdeen Ave SE Kirtland AFB, NM 87117-5776	2 cy